REPORT DOCUMENTATION PAGE

Form Approved
OMB No. 0704-0188

PLEASE DO NOT RETURN YOUR FORM TO THE ABOVE ORGANIZATION.

1. REPORT DATE *(DD-MM-YYYY)*	2. REPORT TYPE	3. DATES COVERED *(From - To)*
01-01-2012	Final Technical Report	01-10-2009 - 01-10-2011

4. TITLE AND SUBTITLE
Miniaturized Retrodirective Arrays for a Nanosatellite Platform

5a. CONTRACT NUMBER
N/A

5b. GRANT NUMBER
N00014-10-1-0056

5c. PROGRAM ELEMENT NUMBER
N/A

6. AUTHOR(S)
Shiroma, Wayne A. (Principal Investigator); Iwami, Reece T. (Graduate Research Assistant); Tonaki, Wade G. (Graduate Research Assistant)

5d. PROJECT NUMBER
N/A

5e. TASK NUMBER
N/A

5f. WORK UNIT NUMBER
N/A

7. PERFORMING ORGANIZATION NAME(S) AND ADDRESS(ES)
University of Hawaii
2530 Dole Street, Sakamaki D-200
Honolulu, HI 96822
(Principal Investigator: Wayne A. Shiroma)

8. PERFORMING ORGANIZATION REPORT NUMBER
N/A

9. SPONSORING/MONITORING AGENCY NAME(S) AND ADDRESS(ES)
Office of Naval Research
875 N. Randolph St.
Arlington, VA 22203-1995
(Program Manager: Dr. Santanu Das, Code 312)

10. SPONSOR/MONITOR'S ACRONYM(S)
N/A

11. SPONSOR/MONITOR'S REPORT NUMBER(S)
N/A

12. DISTRIBUTION/AVAILABILITY STATEMENT
Approved for Public Release. Distribution is Unlimited.

13. SUPPLEMENTARY NOTES
None

14. ABSTRACT
A retrodirective antenna array (RDA) is capable of autonomously steering its radiation pattern toward the source of an interrogating signal, without having prior knowledge of the interrogator location. Integrating an RDA into a mobile platform, such as a nanosatellite, presents unique challenges due to the platform's restrictions in terms of size, weight, and power limitations. This project focused on developing novel RDA architectures that are directly suited for this resource-constrained platform. The three new RDA architectures that were developed during this research project are described. They are based on slope detection, null scanning, and a combination of power detection and null scanning.

15. SUBJECT TERMS
Retrodirective Array, Nanosatellite

16. SECURITY CLASSIFICATION OF:			17. LIMITATION OF ABSTRACT	18. NUMBER OF PAGES	19a. NAME OF RESPONSIBLE PERSON
a. REPORT	b. ABSTRACT	c. THIS PAGE			Wayne A. Shiroma
U	U	U	UU	22	19b. TELEPHONE NUMBER *(Include area code)* 808-956-7218

UNIVERSITY of HAWAI'I® MĀNOA

Final Technical Report

Miniaturized Retrodirective Arrays for a Nanosatellite Platform

Prepared for the Office of Naval Research
Award N00014-10-1-0056
Period of Performance: October 1, 2009 – October 1, 2011

January 1, 2011

20120110335

University of Hawaii at Manoa
2540 Dole Street
Honolulu, HI 96822

Principal Investigator:
Dr. Wayne A. Shiroma
wayne.shiroma@hawaii.edu

Graduate Research Assistants:
Reece T. Iwami
Wade G. Tonaki

1.0 Abstract

A retrodirective antenna array (RDA) is capable of autonomously steering its radiation pattern toward the source of an interrogating signal, without having prior knowledge of the interrogator location. Integrating an RDA into a mobile platform, such as a nanosatellite, presents unique challenges due to the platform's restrictions in terms of size, weight, and power limitations. This project focused on developing novel RDA architectures that are directly suited for this resource-constrained platform. The three new RDA architectures that were developed during this research project are described. They are based on slope detection, null scanning, and a combination of power detection and null scanning.

2.0 Project Overview

The primary objective for the research conducted by the University of Hawaii (UH) through this grant was to support ONR's FORCEnet Vision "... to have the right information, at the right place, at the right time ..." The mobile environment presents many challenges in providing next-generation multimedia (voice, data, imagery) intelligence to warfighters on resource-constrained platforms. By developing miniaturized retrodirective arrays (RDAs) for highly mobile air, surface, land, and subsurface platforms, UH aims to drastically improve the communication capabilities of these so-called "disadvantaged users".

Current antenna systems for high-capacity multimedia communications use a dynamically steered directive beam but require significant increases in size, cost, and complexity over typical omnidirectional antennas. In many cases, highly mobile platforms cannot accommodate the added size, cost, and complexity of the required antenna systems. Therefore, warfighters on these types of platforms are at a severe disadvantage and providing them with the necessary intelligence is of the utmost importance.

An RDA is a class of antenna that provides autonomous steering of a directive beam without requiring complex digital signal processing or knowledge of a user's location. The added directivity of RDAs is achieved with minimal cost and complexity, and can be used to enhance mobile wireless communication system performance, efficiency, and security. UH has developed a miniaturized null-steering RDA that has the potential to provide high-capacity multimedia communications on resource-constrained mobile platforms. This new architecture addresses the drawbacks of previously demonstrated RDAs.

The objectives of the proposed research are:

- Design and develop a prototype miniaturized null-steering RDA for efficient, secure, full-duplex communications.
- Integrate an optimized version of the miniaturized null-steering RDA into a CubeSat bus.

3.0 Introduction

A retrodirective array (RDA) is capable of autonomously steering its radiation pattern toward the source of an interrogating signal [1]. An analog to this type of antenna is a corner reflector,

which reflects a signal back in the same direction as the signal source. Several architectures exist that attain retrodirectivity. The Van Atta array is the simplest, using transmission lines of different length connected between pairs of antenna elements to attain retrodirectivity [2]. Heterodyne mixing arrays use mixers on each element to conjugate the phase of the incoming wave [3]. Other architectures use phase shifters to direct the beam and either phase detectors or power detectors to determine the direction of arrival of the signal [4]-[5].

Higher directivity and the ability to maintain a constant antenna link gain benefits a myriad of mobile applications including low earth orbiting (LEO) satellites, aircraft, and terrestrial vehicles. This research focused on the development of a novel antenna technology for reconnaissance, satellite crosslink, and communications-on-the-move (COTM) applications. The technology is applicable to any space-borne, airborne, seaborne, or terrestrial platform that requires autonomous operation and efficient use of onboard power and computing resources for secure, ad hoc communications. The resource-constrained CubeSat platform was chosen to demonstrate new, resource-efficient RDA architectures.

CubeSats [6] are a class of nanosatellite that have recently experienced rapid growth in the scientific, defense, and academic communities [7]-[9]. Compared to larger, more conventional satellites, CubeSats exhibit a lower cost and shorter development time. Proposed missions often involve clusters of small satellites that form sensor networks, replacing the functionality of a much larger satellite [10]. The challenge in designing such a network – especially a dynamically reconfigurable one – is in establishing and maintaining a reliable crosslink without prior knowledge of their respective locations. Due to their size (1000 cm^3), weight (1 kg), and power (SWaP) limitations, many CubeSats are designed with limited attitude control systems, if at all. Without knowledge of their respective positions, CubeSats must establish and maintain reliable crosslinks between other nodes within the network. RDAs presented a unique solution to these problems [11], which were explored in this research project.

4.0 Retrodirective Array Development

The following sections describe three novel RDA architectures that were developed with support from this grant. First is a slope-detecting array, based on power detection. Next is a null-scanning array, which was the first array to utilize a null in a power-detecting DOA detection scheme. Finally, a CubeSat-optimized version of the null-scanning array, with several hardware and software enhancements built in specifically for the resource-constrained platform in mind.

4.1 Slope-Detecting Array[1]

Most RDAs demonstrated to date are based on analog circuitry with no digital signal processing [3], [12], [13]. The analog nature of these RDAs is appealing because of their resulting simplicity compared to smart antennas. However, because these kinds of arrays must process the interroga-

[1] This section was published in W. G. Tonaki, R. T. Iwami, A. Zamora, T. F. Chun, and W. A. Shiroma, "A Retrodirective Array Using Slope Detection and Phase Shifting," *International Symposium on Antennas and Propagation*, Jeju, Korea, paper A03_1002, Oct. 2010.

tor signal in some fashion to create the retrodirected signal, it causes them to suffer from the limitation of only being able to retrodirect while being interrogated.

This section presents a new all-analog RDA architecture that does not suffer from this limitation. That is, it is able to respond to an interrogating source that does not have to be constantly transmitting. As such, it can respond to pulsed interrogating signals such as those in radar.

The operating concept is as follows. Assume that the RDA is interrogated from some unknown direction. To determine the interrogator's direction of arrival (DOA), the RDA scans the entire visible half-plane while detecting the direction of maximum received power (and thus the DOA). Next, analog control circuitry sets up the phasing that results in a retrodirected beam back in the interrogating direction.

4.1.1 Design

Fig. 1 illustrates the system, which is composed of a phase detector, phase-shifting module, and control circuit. The phase detector, consisting of a maximum-power detecting circuit, determines the DOA. A control circuit then outputs the necessary phase-shifter control voltages that results in a retrodirected beam back in the interrogating direction.

Beam Scanning

Determination of the DOA begins by scanning the entire visible half-plane for RF power. This technique was previously demonstrated in [5], but had to operate in power-detection and retrodirection modes sequentially, rather than simultaneously. It was also only capable of half-duplex communication.

In contrast, the architecture proposed in this section is capable of simultaneously scanning and communicating in full-duplex mode. The DOA determination scheme uses only the two center elements of the array in Fig. 1(a), shown in more detail in Fig. 2. The entire visible half-plane is scanned from $-90° \leq \theta \leq +90°$ for RF power at the 8.1-GHz interrogating frequency, where θ is the scan angle from broadside. Scanning is performed by adjusting V_{scan}, which controls phase shifter PS1, while maintaining $V_{fix} = 0$ V, which fixes phase shifter PS2 to some reference phase. The result is Φ, the phase difference between the two center elements in reference to PS2. PS1 and PS2 are implemented with Hittite HMC538 phase shifters.

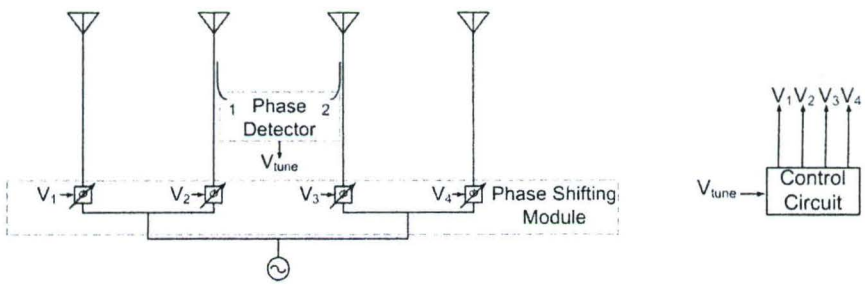

(a) (b)

Fig. 1: Schematic of four-element retrodirective array using a phase detector and phase shifting, showing the three major modules: (a) phase-detector and phase-shifting module, and (b) control circuit.

V_{scan} for PS1 is adjusted via an 8-bit digital counter that iterates through its 256 values and feeds an Analog Devices AD7224 DAC. This provides a 0.7° resolution in θ for a single counter iteration. The DAC outputs a ramp voltage between 0-1.82 V that corresponds to the 0°-360° phase shift Φ applied by PS1.

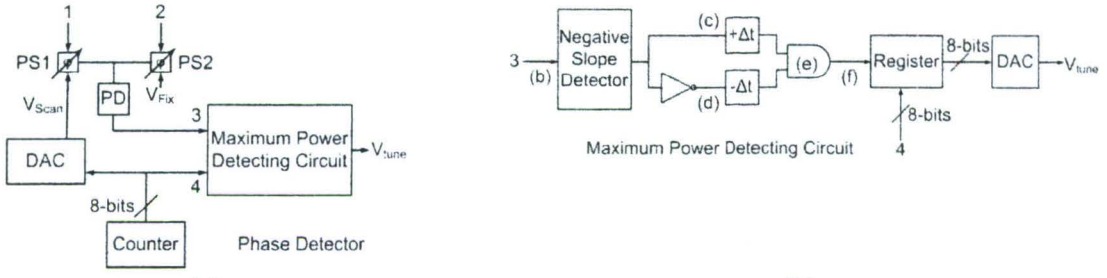

Fig. 2: (a) DOA determination scheme where Ports 1 and 2 correspond to those in Fig. 1(a); (b) Schematic of maximum-power detecting circuit where Ports 3 and 4 correspond to those in Fig. 2(a) and points (b)-(f) correspond to graphs in Fig. 3.

Phase Detection

As the beam formed by the two center array elements scans the visible half-plane, received power at each of those two elements combine through a 2:1 Wilkinson power combiner, and then feed a power detector, which outputs an analog voltage corresponding to the detected RF. The Hittite HMC611 power detector has an inverse relationship between detected power and output voltage. That is, it outputs a DC voltage minimum when detecting maximum RF power over a sweep, and vice versa.

This voltage is fed to the maximum-power detecting circuit shown in more detail in Fig. 2(b), which also receives input from the counter. The maximum-power detecting circuit outputs a voltage V_{tune}, proportional to the phase difference between the two antenna elements (and thus, the DOA). This voltage is used by the control circuit to retrodirect a beam.

Fig. 3 assists in visualizing the DOA determination scheme. Fig. 3(a) shows the DAC ramp signal described earlier. Figs. 3(b)-(f) show the voltages at various points in the schematic of Fig. 2(b), assuming an interrogator located at $\theta = 0°$. At point (b), the power-detecting voltage signal is fed to a negative slope detecting circuit, which outputs an analog voltage value of 5 V when the slope is negative and 0 V when it is positive. The negative slope signal is split into two paths, with one path being digitally inverted; these correspond to points (c) and (d). The two signals are then time-shifted in opposite directions, with one being lagged and the other being led and sent to an AND gate that combines the signals at point (e). The output of the AND at point (f) yields a signal that displays locations where maximum power (and thus the interrogator's DOA) is detected.

Upon finding the maximum power, a Motorola MC74F161A 8-bit register simultaneously loads the corresponding 8-bit counter value that was fed to PS1 to another DAC that outputs a tuning voltage, V_{tune}. This voltage represents the progressive phase shift Φ_p needed for the phase-

shifting module to retrodirect a signal back in the interrogating direction. When not at a maximum power level, the register holds the last known maximum power digital value as V_{tune}. Fig. 1(b) shows that V_{tune} is fed to a control circuit, which then outputs four voltages V_1-V_4 that control the phase shifters that steers a retrodirected signal back to the interrogator.

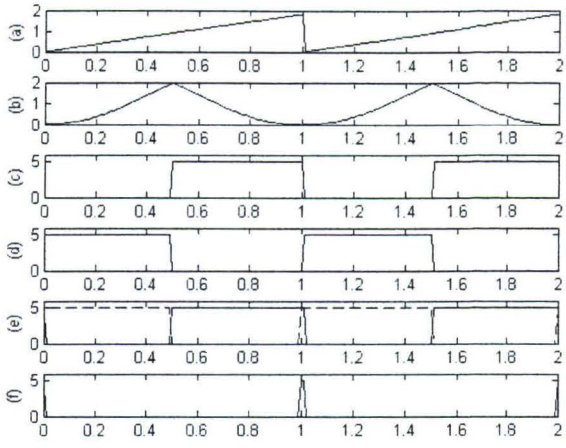

Fig. 3: Voltages at various points of the maximum-power detecting circuit of Fig. 2(b), assuming an interrogator located at $\theta = 0°$. X-axis units are in periods. Y-axis units are in volts. (a) ramp voltage controlling PS1 representing a 0°-360° phase shift Φ; (b) power detector voltage; (c)-(e) signals manipulated from (b); (f) maximum power detection.

Phase-Shifting Module

Fig. 1(a) shows the phase-shifting module, where an LO at 8.19 GHz feeds a 1:4 Wilkinson power divider that feeds four parallel HMC538 phase shifters, then four quasi-Yagi antenna elements. The phase-shifting module uses

$$\Phi_p = \frac{2\pi}{\lambda} d \sin\theta \quad , \tag{1}$$

where Φ_p is the progressive phase difference between the antenna elements, d is the antenna element spacing, and λ is the interrogating wavelength.

The phase detector and phase-shifting module are integrated to eliminate the need for separate transmit and receive circuitry. They share a 4-element quasi-Yagi array with a 6.0 – 8.7 GHz bandwidth (37% fractional bandwidth). The transmit and receive frequencies are 8.19 and 8.10 GHz, respectively. The array is fabricated on Rogers TMM10i (thickness = 1.016 mm, $\varepsilon_r = 9.8$) and features half-wavelength spacing at 7.82 GHz.

4.1.2 Experimental Results

Tracking Capability

Fig. 4(a) shows the monostatic transmit and receive radar cross section (RCS) pattern of the RDA. The plots demonstrate the RDA's active tracking capabilities across its visible range. The transmit setup involved two horns collocated on a sweeping arm that was swept from $-40° \leq \theta \leq 40°$. One horn interrogated the RDA at 8.10 GHz, while the other horn received the transmitted response of the RDA at 8.19 GHz. The receive setup used a transmitting horn swept across -40°

$\leq \theta \leq 40°$ while power received at the RDA was recorded. The -10 dB dips between -30° and -20° are due to the introduction of additional peaks in Fig. 3(f) that affected the steering of the RDA.

Full-Duplex Operation

Full-duplex operation of the RDA was demonstrated by taking bistatic patterns in both receive and transmit modes. Transmit RCS patterns involved using a static 8.1 GHz interrogating horn, and a second horn, mounted on a rotating arm that is swept from $-60° \leq \theta \leq 60°$, measuring the received power from the RDA transmitting at 8.19 GHz. For the receive RCS patterns, an interrogating horn at 8.1 GHz was fixed and the DOA was determined by the RDA. The register was forced into a hold state, keeping the RDA pointing in the same direction, while an 8.19 GHz transmitting horn was swept from $-60° \leq \theta \leq 60°$. Power received at the RDA was recorded. Experimental transmit and receive RCS patterns are reported in Fig. 4 for interrogating locations of -10°, 0°, and 30°. There is good agreement with the theoretical plots and the experimental plots that highlight the RDA's accurate retrodirective abilities.

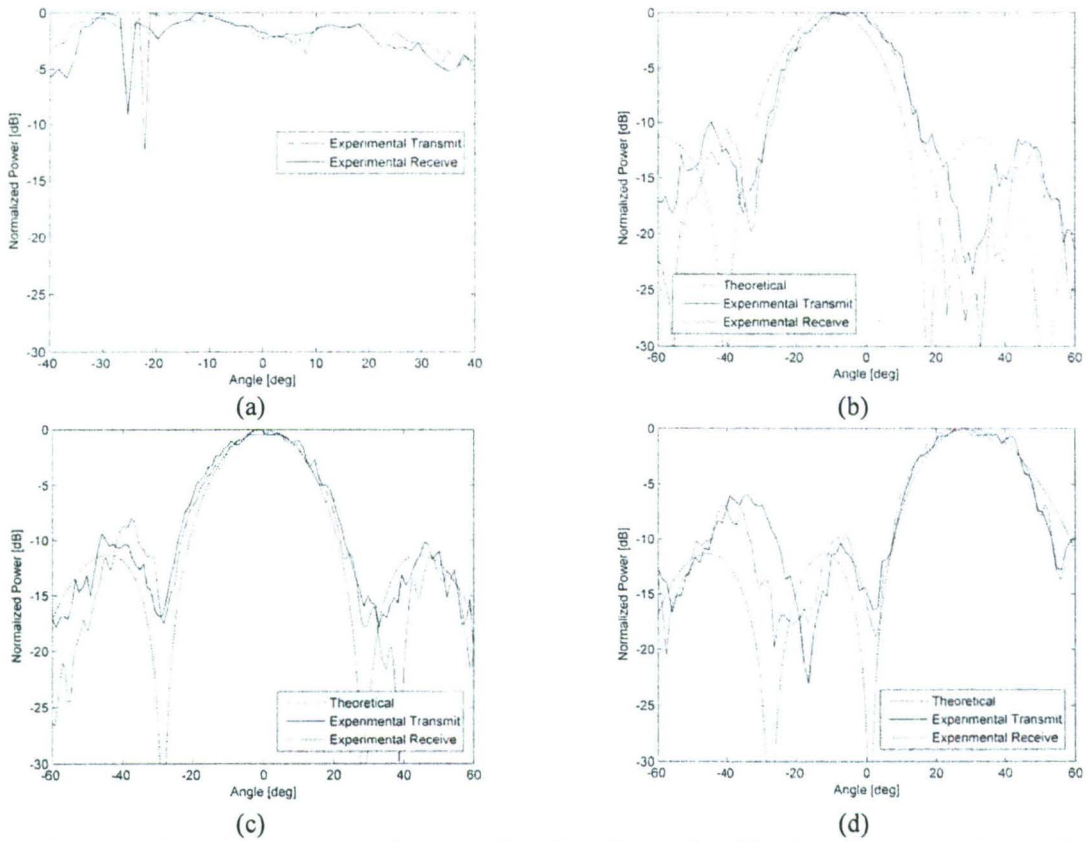

Fig. 4: (a) Monostatic radar cross section for transmit and receive modes; Bistatic radar cross sections with interrogator at: (b) -10°, (c) 0°, and (d) +30°. Proper transmit and receive frequency operation demonstrates full-duplex capability.

4.2 Null-Scanning Array[2]

Several types of RDAs have been demonstrated recently, each with distinguishing characteristics, e.g. [12], [13]. In general, most of these architectures require increasing the array size to increase the DOA resolution accuracy. The array described in this section increases the DOA resolution without increasing the array size by employing null scanning.

Our null-scanning RDA is an evolution of the beam-scanning RDA [5], in which a beam is scanned across a steering range, and the DOA is determined from the angle for which maximum power is detected. A drawback to this design is that constant target tracking cannot be achieved because the array must switch between power-detection and communication modes. Also, the half-duplex communication system inherently does not accommodate simultaneous transmission and receive capabilities.

This section presents a full-duplex RDA that uses a null rather than a beam to determine DOA. As a null is scanned throughout the angular range, the received power is recorded in the same manner as in [5]. In contrast to beam scanning, the DOA of the interrogator is determined by the angle for which the power received by the null-steering array is a minimum. This information can then be used by a microcontroller to steer the beam of the full-duplex phase-shifting array in the direction of the interrogator. Near the interrogator's angular direction, the rate of change of received power is much greater in null-steering mode when compared to an identically sized array using beam steering.

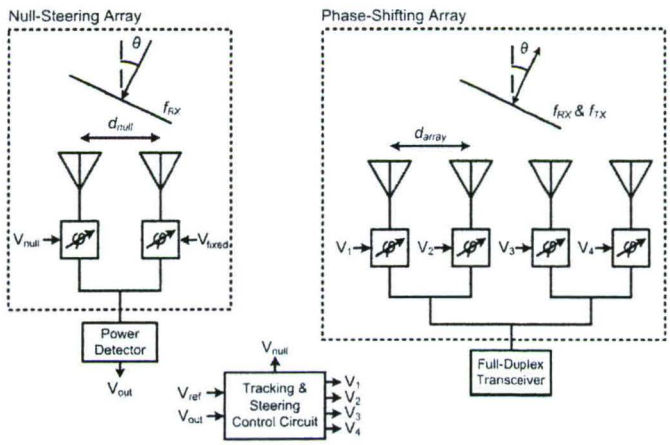

Fig. 5: Schematic of the null-steering, phase-shifting array.

4.2.1 Design

The self-steering array architecture is comprised of two sub-arrays: a two-element null-steering array, and a full-duplex phase-shifting array, as shown in Fig. 5. The null-steering array uses a power-detection scheme to determine the DOA of an interrogator signal. This information is

[2] This section was published in R. T. Iwami, A. Zamora, T. F. Chun, M. K. Watanabe, and W. A. Shiroma, "A retrodirective null-scanning array," *Microwave Symposium Digest (MTT), 2010 IEEE MTT-S International*, pp.81-84, 23-28 May 2010.

used to properly phase each element in an adjacent phase-shifting array to steer a beam in the direction of the interrogator. The two sub-arrays are interfaced and controlled by an RF power-detecting circuit and an analog operational amplifier control circuit.

Null-Steering Array

Fig. 5 shows the schematic of the two-element null-steering array. The array is comprised of two $\lambda/2$-spaced patch antenna elements, fabricated on Rogers RO4350B (thickness = 1.524 mm, ε_r = 3.66) for 7.31-GHz operation. A Hittite HMC538 phase shifter controls the phasing of each element, with one static and one varying, causing a null to scan across the $-90° \leq \theta \leq 90°$ sweep range. A 2:1 Wilkinson power combiner combines the received signals at the two elements as the input to the RF power-detecting circuit.

The null of a two-element array pattern can be steered by varying the phase difference, φ_{pnull}, between antenna elements. Based on an array spacing of $d = \lambda/2$, φ_{pnull} as a function of steering angle θ is given by:

$$\varphi_{pnull} = \frac{2\pi}{\lambda} d \sin\theta - \pi = \pi \sin\theta - \pi. \tag{2}$$

The additional $-\pi$ term in (2) corresponds to the 180° phase difference between elements which produces a null. The null-steering array establishes the required phase difference by fixing one phase shifter (PS1) in an initial state, while varying the phase of the other (PS2) according to (2) for a desired angle θ. A linear fit approximates PS2's characteristic curve, which is used by the null-steering control circuit to scan the null. The linear fit is also used by the RF power-detecting circuit to calculate the direction of the interrogator.

RF Power-Detecting Circuit

Fig. 6 shows a schematic of the RF power-detecting circuit. This module utilizes a Hittite HMC602 RF power detector to convert a received power measurement into a proportional analog DC voltage. A PIC microcontroller with built-in ADC inputs reads in the analog voltage and stores each value as an 8-bit digital representation in a 256-byte array. The 256 values allows for 0.7° steering resolution, assuming a $-90° \leq \theta \leq 90°$ steering range. The PIC keeps track of the angle where minimum power is detected, which corresponds to the direction of the interrogator when using a null-steering approach. The PIC then outputs a voltage corresponding to the phase difference between elements required to point a beam in the direction of the interrogator with the phase-shifting array.

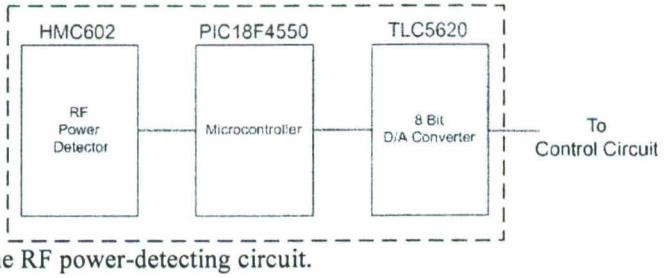

Fig. 6: Block diagram of the RF power-detecting circuit.

Full-Duplex Phase-Shifting Array

Fig. 5 shows the schematic of the full-duplex phase-shifting array. Full-duplex operation enables simultaneous transmit and receive channels, which is implemented by utilizing separate transmit and receive frequencies. A four-element patch array was fabricated using $\lambda/2$-spaced antenna elements fabricated on Rogers RO4350B. This design assumes that the interrogator signal received by the null-steering array is also the received signal of interest. Therefore, the array shares the same receive frequency of 7.31 GHz, with a transmit frequency of 7.33 GHz. Four Hittite HMC538 phase shifters connect to the four antenna elements, which then pass the received RF through a 4:1 Wilkinson power combiner. The output is fed to an LO (transmit) or spectrum analyzer (receive) for testing purposes, which would be replaced by a matched transceiver in a full prototype design.

The phase-shifting array uses a similar phase-progression-to-steering-angle relationship as the null-steering array, but without the additional $-\pi$ term. This allows beamsteering at a given angle θ, again assuming $\lambda/2$-spaced elements:

$$\varphi_p = \frac{2\pi}{\lambda} d \sin\theta = \pi \sin\theta. \tag{3}$$

The control voltage versus phase shift characteristic curve is comprised of the average of all four phase shifters, and a linear approximation is used to define the function. The linear fit is used by the control circuit to properly phase each element based on the input from the RF power-detecting circuit. The required phase shift, φ_s, is approximated by:

$$\varphi_s \approx S V_{ctl}, \tag{4}$$

where S [deg/V] is the calculated sensitivity of the phase shifter, given by the slope of the linear fit line.

The phase shifter sensitivity value of $S = 221.4$ deg/V yields a voltage range from 0 V – 2.44 V, corresponding to a phase shift of 0° – 540° degrees, respectively. This range is required to provide a maximum phase difference between elements of ±180°. Using this maximum phase difference and rearranging (3) to solve for θ_{max}, the maximum beam-steering angles are:

$$\theta_{max} = \sin^{-1}\left(\frac{\pm\pi}{\pi}\right) = \pm 90°, \tag{5}$$

which covers the entire visible half-plane.

Control Circuit

The control circuit takes the output from the RF power-detecting circuit, which is a voltage corresponding to a desired phase shift ranging from ±180°, and outputs four voltages, V_1-V_4, which feed the phase shifters of the phase-shifting array. If φ_{ref} is taken to be the reference phase at the center of the four-element array, there will be a $-3\varphi_p/2$, $-\varphi_p/2$, $+\varphi_p/2$, $+3\varphi_p/2$ phase progression between elements 1 – 4.

A first-stage op-amp network provides a voltage shift operation, yielding a voltage V_p ranging from -0.85 V to +0.85 V. Another op-amp network takes this voltage along with the calculated value of V_{ref}= 1.22 V, derived from (4) and given by:

$$V_{ref} = \frac{\varphi_{ref}}{S} = \frac{270°}{221.4°/V} \tag{6}$$

to produce the required phase shifter voltages, V_1-V_4, corresponding to the φ_p phase progression mentioned above.

4.2.2 Experimental Results

Null-Steering Versus Beam-Steering Comparison

The first experiment tests the assertion that a null-steering array based on minimum power searching provides greater DOA resolution than a similarly sized beam-steering array based on maximum power searching. Using the two-element patch-antenna array that was designed for the null-steering sub-array, a beam was swept over the visible range from -90° ≤ θ ≤ 90°, while received power was recorded. Based on the relative phase shift applied by the phase shifter PS2, the corresponding null angles were calculated by rearranging (2):

$$\theta_{null} = \sin^{-1}\left(\frac{\phi_{pnull} + \pi}{\pi}\right). \tag{7}$$

Figs. 7 and 8 show power received versus steering angle for an interrogator at θ = 0° and θ = +50°, respectively. The vertical dashed line in each plot denotes the location of the interrogator. For the null-steering configuration, the interrogator location is interpreted as the angle for which minimum power is detected. In the beam-steering configuration, the location is taken as the angle where maximum power is detected.

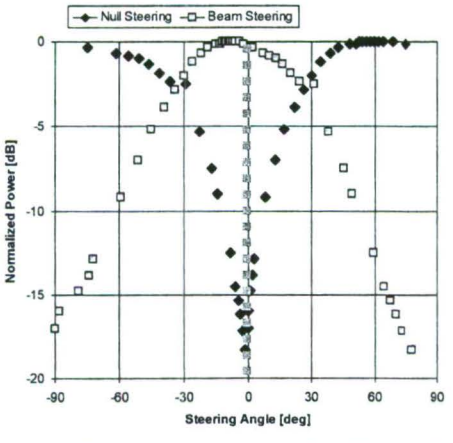

Fig. 7: Power received versus steering angle for an interrogator at θ = 0°. A null-steering array produces a 1.3° error, while a beam-steering array produces a 4°-12° error range.

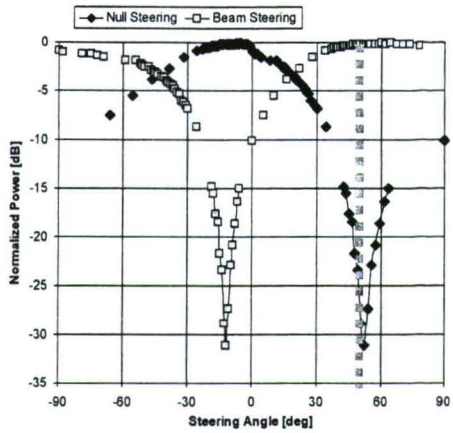

Fig. 8: Power received versus steering angle for an interrogator at $\theta = +50°$. A null-steering array produces a 2.4° error, while a beam-steering array produces a 10°-14° error range.

This experiment confirms the superior resolving power of the null-steering array due to the greater rate of change in received power near the interrogator's angular direction compared to the beam-steering array. The plots show that the null-steering array exhibits less steering-angle error than the beam-steering array. The narrow null "beamwidth" also yields a single-angle value from the power-detecting circuit, as opposed to the beam-steering setup which produces a range of qualifying yet incorrect angles due to its broad beamwidth. This precision assists the system in stabilizing and pointing at a particular angle, rather than randomly shifting between values.

Tracking Capability

Fig. 9 shows the monostatic radar cross section (RCS) pattern of the RDA. The setup included two horns stationed on a sweeping arm swept from $-60° \leq \theta \leq 60°$. One horn interrogated the RDA at 7.31 GHz, while the other collocated horn received the RDA's transmitted response at 7.33 GHz. The plot shows that the RDA tracks the interrogator as it sweeps across the visible range.

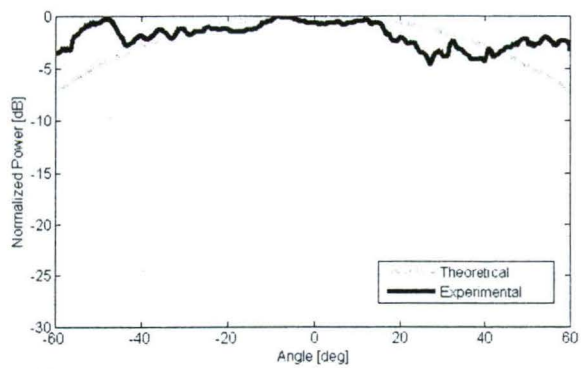

Fig. 9: Monostatic radar cross section.

Full-Duplex Operation

To show the full-duplex operation of the RDA, bistatic RCS patterns were taken in both receive and transmit modes. For the transmit RCS patterns, a static 7.31-GHz interrogating horn is fixed, while a second horn, mounted on a rotating arm, is swept from $-60° \leq \theta \leq 60°$ measuring re-

ceived power from the RDA transmitting at 7.33 GHz. For the receive RCS patterns, a 7.31-GHz interrogating horn is fixed, and the corresponding V_p voltage is recorded. Subsequently the phase shifter control circuit was disconnected from the power-detecting block and the phase shifter control circuit was directly fed the recorded voltage, V_p. A 7.33-GHz transmitting horn was then swept from $-60° \leq \theta \leq 60°$ while the RDA measured received power levels. Resulting transmit and receive RCS patterns are reported for interrogator locations of -30°, 0°, and +10° (Fig. 10).

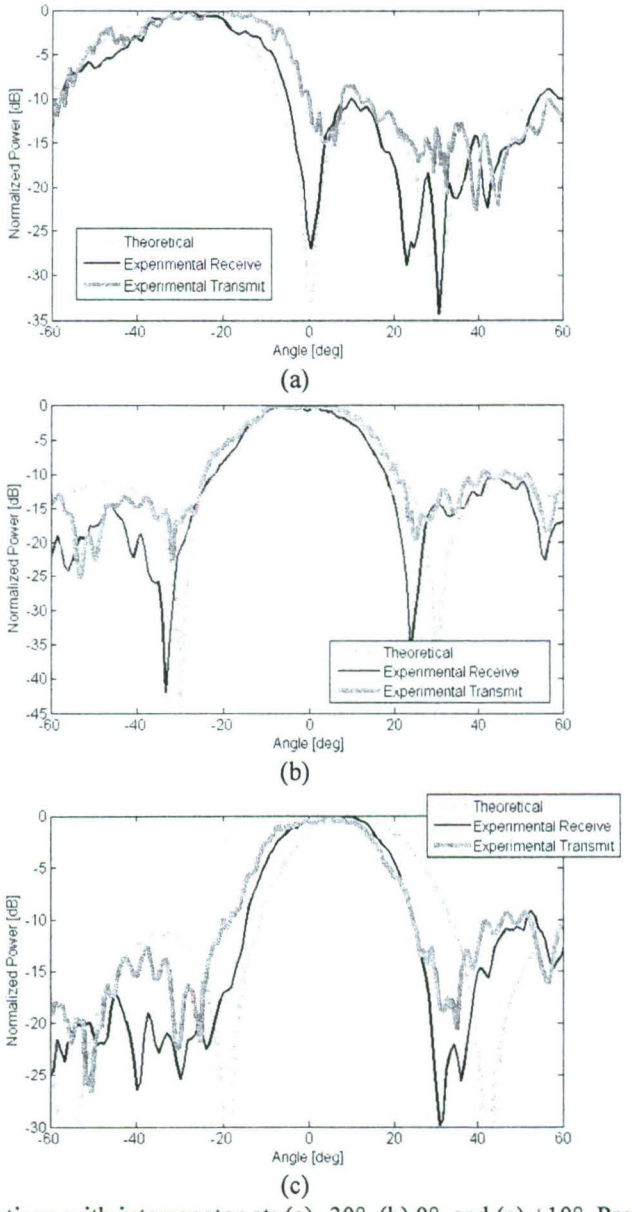

Fig. 10: Bistatic radar cross sections with interrogator at: (a) -30°, (b) 0°, and (c) +10°. Proper transmit and receive frequency operation shows full-duplex capability.

4.3 Small-Satellite-Optimized Array[3]

This section presents the development of a new RDA architecture designed specifically for the resource-constrained CubeSat platform. Although retrodirective arrays have been in development for the past 50 years [2], [3], integrating an RDA into a CubeSat represents a challenge due to the strict SWaP requirements. The first RDA developed for a CubeSat platform [14], [15] achieved retrodirectivity using the heterodyne technique [10], where mixers are used to phase conjugate the received signal. The biggest drawback to this type of RDA architecture is that the signal strength at the output of the array is dependent on the incoming signal strength, and thus the distance from the interrogator. The path loss is proportional to R^4, where R is the distance between communicating nodes [16].

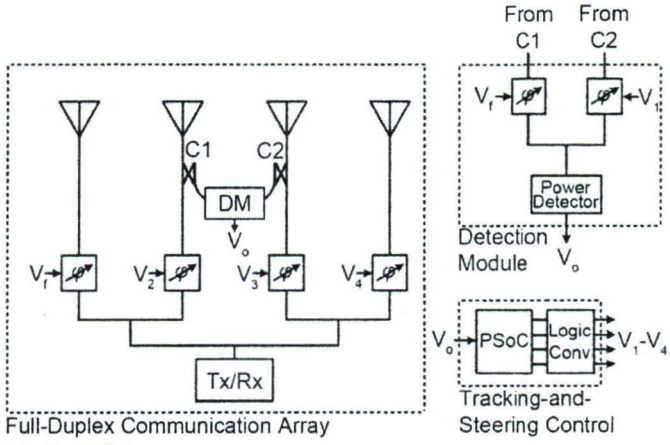

Fig. 11: Schematic of the CubeSat RDA.

The null-scanning RDA of [17] was developed to address the R^4 path loss issue by utilizing a power-detection approach, thereby decoupling the received and transmitted signals, and achieving an R^2 path loss. It was shown that by utilizing a null for minimum power detection, a two-element microstrip patch array was much more capable in resolving an interrogator signal's direction-of-arrival (DOA) when compared to an identically equipped beam-steering RDA. The CubeSat RDA described in this section utilizes this null-scanning approach for its benefits in retrodirected path loss and array minimization, and improves on the architecture with several SWaP-motivated hardware and software optimizations.

4.3.1 Design

Fig. 11 shows the schematic of the CubeSat RDA, which consists of three principal modules: a single four-element array for both DOA estimation and transceiver communications, a power-detection module to determine the DOA of the interrogating signal, and a tracking-and-steering control module that outputs the necessary control voltages to steer the beam of the four-element array in the direction of the interrogator. The DOA detection module and tracking-and-steering

[3] This section was submitted for review to *IEEE Antennas and Wireless Propagation Letters* in R. T. Iwami, W. G. Tonaki, T. F. Chun, and W. A. Shiroma, "A Power-Detecting, Null-Scanning, Retrodirective Array for a 1.5U CubeSat Platform," Dec. 2011.

control module are interfaced to provide autonomous, self-steering capability to the four-element array.

Detection and Communication Array

The antenna array is comprised of four $\lambda/2$-spaced microstrip patch antenna elements, fabricated on Rogers RT/Duroid 6002 substrate (thickness = 0.762 mm, $\varepsilon_r = 2.94$). This substrate was chosen for its low dielectric loss. The frequencies of operation chosen were 9.59 GHz for transmit and 9.67 GHz for receive in full-duplex communication.

In contrast to the architecture in [17], which uses one array for DOA detection and another array for transmit communications, the architecture in Fig. 11 combines both functions into one array. This is achieved by siphoning off one-tenth of the received interrogator signal power from the two central antenna elements using 10-dB couplers. Combining the detection and communication arrays not only reduces the physical size of the array, but also improves the steering accuracy as both arrays are collocated at their centers, rather than being laterally offset from each other [17].

DOA Detection Module

The DOA detection module determines the direction of arrival of an interrogating signal. The array utilizes the null-scanning approach for power detection, first presented in [17]. This information is then used by the control module to retrodirect a signal back to the interrogator. DOA detection is accomplished using two phase shifters that steer a receive null formed by the two central elements of the antenna array. Received RF signal power is recorded at each angle steered. The DOA of the interrogator signal is then computed by finding the angle for which minimum power is received.

The DOA detection module consists of two Hittite HMC543LC4B digital phase shifters, a 2:1 Wilkinson power combiner, and a Hittite HMC611LP4 logarithmic RF power detector.

The 4-bit, 16-state Hittite HMC543LC4B digital phase shifter provides full 360° phase coverage. The four bits offer 22.5° phase resolution, which translates to roughly 7° of steering resolution that decreases as one steers farther from broadside.

Compared to the analog phase shifters used in previous designs [5], [17], [18] the discrete nature of digital phase shifters resulted in tolerance to small variations in control voltage, which are inherent in any control circuit. The analog phase shifters used previously were extremely sensitive at 221.4 deg/V [17], where commonly occurring variations in control voltages on the order of tenths and hundredths of volts would cause steering angle errors and instability. Thus, the use of digital phase shifters allows for increased phase stability and steering angle accuracy and precision.

Tracking-and-Steering Control Module

PSoC 5

The processing unit of the RDA uses Programmable System-on-Chip (PSoC) technology. The PSoC 5 is a software-configured device with a built-in microcontroller unit (MCU) and mixed-signal array [19]. The PSoC 5 functions primarily as a microcontroller: executing the tracking-and-steering control algorithm, referencing a lookup table for phase shifter control, and outputting the necessary digital control signals to steer the detection and communication array. Table I shows an abbreviated lookup table displaying the necessary logic values for each bit of all phase shifters in the RDA. A PSoC analog signal block is configured as an analog-to-digital converter (ADC), to digitize the analog signal received from the DOA detection module.

TABLE I
ABBREVIATED CONTROL MODULE LOOKUP TABLE

θ	PS2				PS3				PS4			
	B4	B3	B2	B1	B4	B3	B2	B1	B4	B3	B2	B1
30.00	1	1	0	0	1	0	0	0	0	1	0	0
22.02	1	1	0	1	1	0	1	0	0	1	1	1
14.48	1	1	1	0	1	1	0	0	1	0	1	0
7.18	1	1	1	1	1	1	1	0	1	1	0	1
0.00	0	0	0	0	0	0	0	0	0	0	0	0
-7.18	0	0	0	1	0	0	1	0	0	0	1	1
-14.48	0	0	1	0	0	1	0	0	0	1	1	0
-22.02	0	0	1	1	0	1	1	0	1	0	0	1
-30.00	0	1	0	0	1	0	0	0	1	1	0	0

Detection Stabilizer Algorithm

To stabilize the power detection readings, an averaging process was implemented. A "super-sweep" was comprised of 256 total power readings stored in a 256-entry array. For each steering angle, five individual power readings were taken. To allow for the RF power detector to settle after a state change, the first of the five power readings was discarded. This resulted in 64 data entries over the 16 steering angles, which made up one sub-sweep. Four of these sub-sweeps were performed to collect the 256 data entries of a single super-sweep. The 16 entries for each steering angle were then averaged to create a 16-element array of averaged power levels representing the 16 different steering angles. The null-steering DOA detection algorithm was then run on this 16-element averaged array, where the angle for which minimum power detected was selected as the direction of the interrogator. The detection algorithm takes 250 milliseconds to determine the DOA of the interrogator and retrodirect a response

Retrodirected Response

With the DOA of the interrogator signal determined, the control module then steers a communication beam with the four-element array towards that angular direction. Using the lookup table stored in the PSoC, the control module outputs the necessary bit values that correspond to a par-

ticular angular direction. The communication array is controlled by bit values in columns PS2, PS3, and PS4 of Table I.

4.3.2 Experimental Results

Full-Duplex Operation

To show the full-duplex operation of the RDA, bistatic RCS patterns were taken in both receive and transmit modes. For the bistatic RCS patterns, a static 9.67-GHz interrogating horn was fixed at a particular angle, while a second horn, mounted on a rotating arm, was swept from -60° $\leq \theta \leq$ 60° measuring the RDA response. Resulting transmit and receive RCS patterns are reported for three separate angles between -40° $\leq \theta \leq$ 50°, shown in Fig. 12 (a)-(c).

The patterns show good agreement with theoretical plots over a wide range of angles, as both transmit and receive main beams and sidelobes are formed in their appropriate angular directions and magnitudes. The use of digital states with binary control voltages provides this stability. The detection stabilizer algorithm also improved performance of the tracking-and-steering control module. Readings of the output voltage from the RF power detector improved from variances of tenths of a volt down to the order of millivolts, enabling greater precision in interrogator detection.

Interrogator Tracking Capability

The setup for the monostatic RCS pattern consisted of two co-located horns swept from -60° $\leq \theta \leq$ 60°. One horn interrogated the RDA at 9.67 GHz, while the other received the RDA's transmitted response at 9.59 GHz. Fig. 13 shows the monostatic RCS pattern of the RDA. The theoretical plot shows the radiation pattern of a single microstrip patch element, which is the ideal case of a monostatic RCS pattern of an RDA. The experimental plot shows that the RDA tracks the interrogator as it sweeps across the visible range, with good agreement with the theoretical plot.

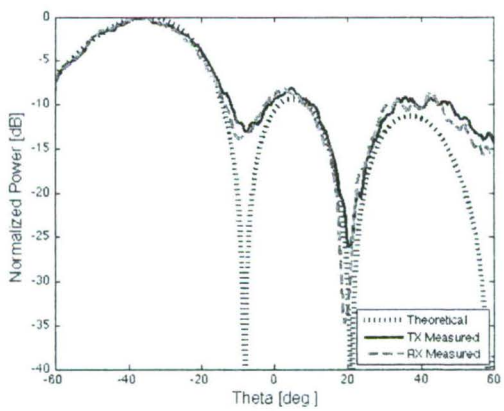

(a)

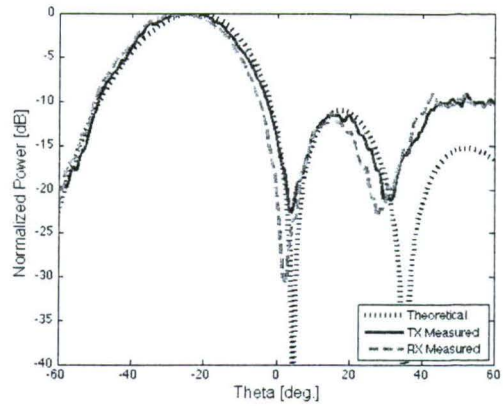

(b)

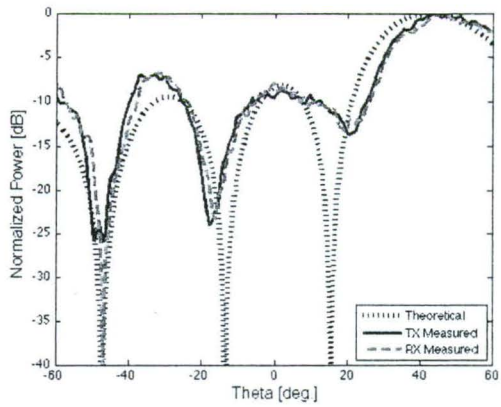

(c)

Fig. 12: Bistatic RCS measurements with interrogator at: (a) -40°, (b) -25°, and (c) +50°. Proper transmit and receive frequency operation shows full-duplex capability.

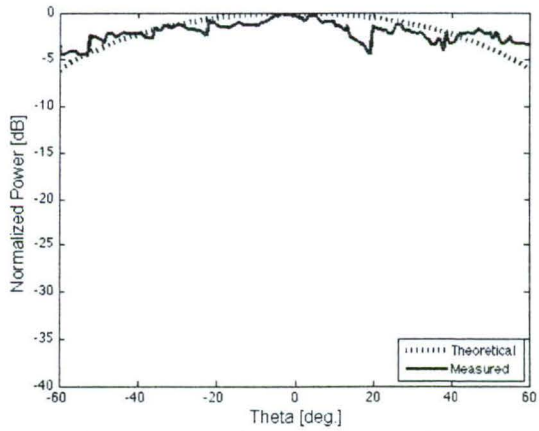

Fig. 13: Monostatic RCS measurement showing proper interrogator tracking by the RDA.

4.3.3 CubeSat Prototype

The results shown in the previous section were collected with a breadboard implementation of the RDA and control circuitry. As part of the ongoing progress of this project, a prototype model of the RDA was developed for future integration with other CubeSat electrical and mechanical subsystems, consisting of solar arrays, batteries, thermal control unit, command and control, and

telemetry. The four-element, 1-D RDA was designed to fit within a 1.5U CubeSat structure, which measures 10 cm x 10 cm x 15 cm, with a mass of no more than 1.5 kg. The design consisted of two four-layer printed circuit boards (PCBs): one dedicated to full-duplex communication, the other for power detection. Fig. 14 shows the assembled CubeSat prototype with dimensions of 4 cm x 10 cm x 14 cm. The RDA hardware has a mass of 186 g.

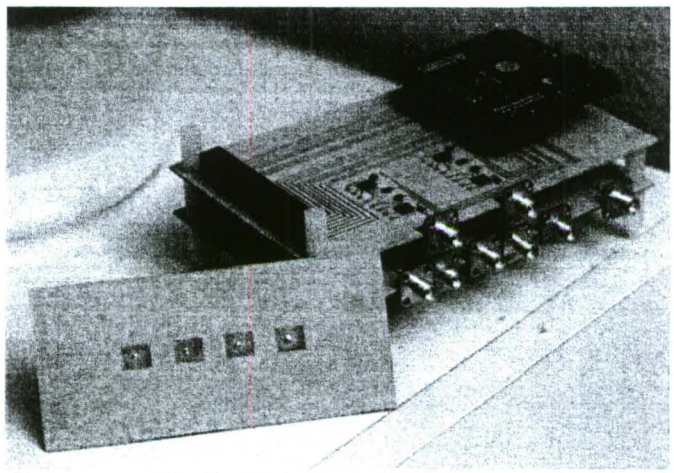

Fig. 14: Prototype of the null-scanning, CubeSat RDA. Assembled control circuitry dimensions: 4 cm x 10 cm x 14 cm. Antenna array dimensions: 10.5 cm x 4.75 cm.

The two boards were interfaced by the CubeSat Stackable Interface (CSI) for digital and power signals, and SMA-connectorized tensolite cables for RF signals. The CSI serves as the basis of the satellite's CDH architecture [20]. CSI minimizes the need for a complex wiring scheme to distribute voltages across a PCB stack by providing standardized voltages across a common bus. CSI uses the PCI-104 standard that not only provides a robust connection, but also fits within a 1U CubeSat form factor. A key feature of CSI is the option to place addressable I/O expanders on each board in the stack to be accessed by an I2C bus, which allows for remote access for a multitude of I/O in the system. The further addition of on/off switches controlled by this I/O expander allows for a remote power management system that is controlled by two lines across CSI as shown in Fig. 15.

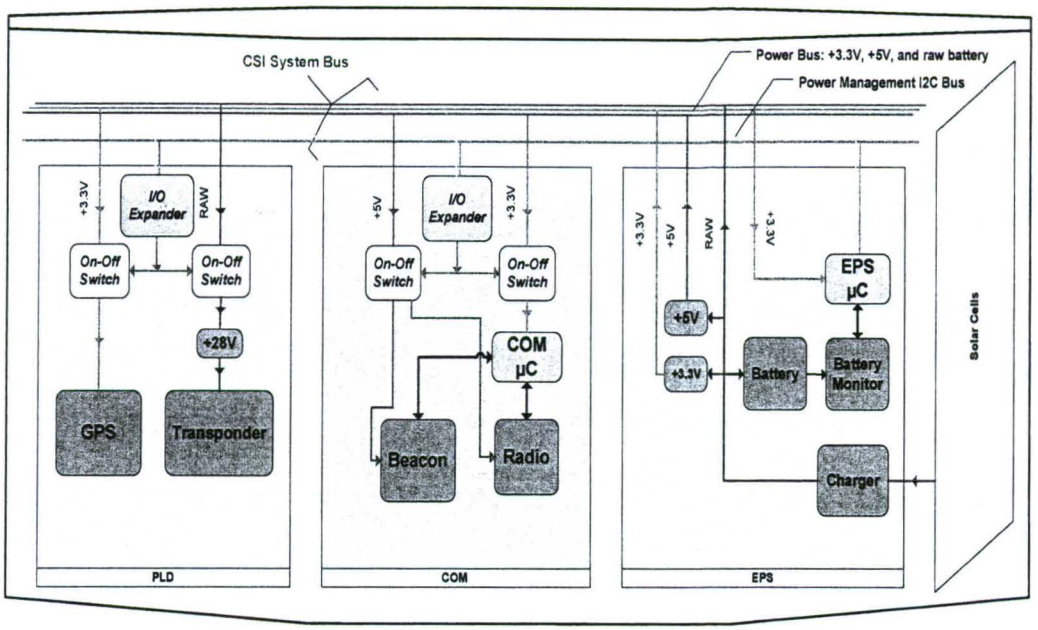

Fig. 15: Block diagram of CSI architecture.

Table II shows that the DC power consumption of the various components of the CubeSat RDA prototype is 1 W, which is well within the power-generation capabilities of CubeSats equipped with either body-mounted or deployable solar panels, together with batteries for operation in eclipse [21], [22]. This figure shows much promise for future RDA-CubeSat missions.

TABLE II
CUBESAT RDA MODEL DC POWER CONSUMPTION

Description	Quantity	Power [W]
HMC543LC4B Phase Shifter	6	0.000
HMC564LC4 LNA	2	0.306
HMC611LP4 Power Detector	1	0.53
7404 Hex Inverter	12	0.144
PSoC 5	1	0.03
Total		1.01

5.0 Conclusion

Integrating a retrodirective array and a small-satellite, like a CubeSat, presents unique challenges due to the platform's restrictions in terms of size, weight, and power limitations. This project focused on developing novel RDA architectures that are directly suited for this resource-constrained platform. Three novel RDA architectures were developed and tested, with design and measurement results presented. The slope-detecting array was based on power detection, and could respond to an interrogating source that did not have to be constantly transmitting. The null-

scanning array was the first array to utilize a null in a DOA detection scheme. Finally, a CubeSat-optimized version of the null-scanning array was presented. This array had several hardware and software enhancements built in specifically for the resource-constrained platform. A prototype design for a 1.5U CubeSat RDA that interfaced with the UH CSI bus was also presented.

6.0 References

[1] W. A. Shiroma, R. Y. Miyamoto, G. S. Shiroma, A. T. Ohta, M. A. Tamamoto, and B. T. Murakami, "Retrodirective Systems," *Encyclopedia of RF and Microwave Engineering*, K. Chang, Ed. Hoboken, NJ: Wiley-Interscience, 2005, vol. 5.

[2] L. C. Van Atta, *Electromagnetic Reflector*, U.S. Patent 2,908,002 (1959).

[3] C. Y. Pon, "Retrodirective array using the heterodyne technique," *IEEE Trans. Anten. Propag., AP-12:176–180* (1964).

[4] G. S. Shiroma, R. Y. Miyamoto, and W. A. Shiroma, "A 16-element two dimensional active self-steering array using self oscillating mixers," *IEEE Trans. Microwave Theory Tech., 51:2257–2264* (2003).

[5] J. A. Akagi, A. Zamora, M. K. Watanabe, and W. A. Shiroma, "A self-steering array using power detecting and phase shifting," *IEEE MTT-S Int. Microwave Symp. Dig.*, pp. 1325-1328, June 2008.

[6] H. Heidt, J. Puig-Suari, A. S. Moore, S. Nakasuka, R. J. Twiggs, "CubeSat: a new generation of picosatellite," in *Proc. 14th Annual AIAA/USU Conf. on Small Satellites*, Logan, UT, Aug. 2001.

[7] K. Woellert, P. Ehrenfreund, A. J. Ricco, and H. Hertzfeld, "Cubesats: Cost-effective science and technology platforms for emerging and developing nations," *Advances in Space Research*, vol. 47, no. 4, pp. 663-684, Feb. 2011.

[8] W. A. Shiroma, L. K. Martin, J. M. Akagi, J. T. Akagi, B. L. Wolfe, B. A. Fewell, and A. T. Ohta, "CubeSats: A Bright Future for Nanosatellites," *Central European Journal of Engineering*, vol. 1, no. 1, pp. 9-15, Mar. 2011.

[9] L. David, "Small satellites prompt big ideas for next 25 years," Space.com, Oct. 2011, http://www.space.com/13283-small-satellites-cubesats-research-technology.html.

[10] C. J. McNutt, "Modular Nanosatellites – Plug-and-play (PnP) CubeSat," in *7th Responsive Space Conf.*, pp. 1-14, Apr. 2009.

[11] R. T. Iwami, Bao Jun Lei, T. Lim, W. G. Tonaki, T. F. Chun, A. Zamora, J. C. Longhi, M. K. Watanabe, J. M. Akagi, W. A. Shiroma, "Miniaturization challenges for autonomously phased arrays in a CubeSat application," *Wireless Information Technology and Systems (ICWITS), 2010 IEEE International Conference on*, Aug. 2010.

[12] G. S. Shiroma, R. Y. Miyamoto, and W. A. Shiroma, "A full-duplex dual-frequency self-steering array using phase detection and phase shifting," *IEEE Trans. Microw. Theory Tech.*, vol. 54, no. 1, pp. 128-134, Jan.2006.

[13] T. Brabetz, V. F. Fusco, and S. Karode, "Balanced subharmonic mixers for retrodirective-array applications," *IEEE Trans. Microw. Theory Tech.*, vol. 49, no. 3, pp. 465-469, Mar. 2001.

[14] B. T. Murakami, M. A. Tamamoto, A. T. Ohta, G. S. Shiroma, R. Y. Miyamoto, and W. A. Shiroma, "Self-steering antenna arrays for distributed picosatellite networks," *Proc. 17th Annu. AIAA/USU Small Satellites Conf.*, 2003.

[15] B. T. Murakami, J. D. Roque, S. S. Sung, G. S. Shiroma, R. Y. Miyamoto, and W. A. Shiroma, "A quadruple subharmonic phase-conjugating array for secure picosatellite cross-links," in *2004 IEEE MTT-S Microw. Symp. Dig.*, Fort Worth, TX, June 2004, pp.1687-1690.

[16] G. S. Shiroma, "Security enhancement and path loss minimization of retrodirective arrays for wireless communications networks," Ph.D. dissertation, University of Hawaii, Honolulu, HI, Dec. 2007.

[17] R. T. Iwami, A. Zamora, T. F. Chun, M. K. Watanabe, and W. A. Shiroma, "A retrodirective null-scanning array," in *IEEE MTT-S Int. Microw. Symp. Dig.*, Anaheim, CA, pp.81-84, May 2010.

[18] A. Zamora, M. K. Watanabe, J. M. Akagi, T. F. Chun, and W. A. Shiroma, "An inter-element phase-detecting retrodirective array for nonuniform wavefronts," in *IEEE MTT-S Int. Microw. Symp. Dig.*, Boston, MA, pp. 817-820, Jun. 2009.

[19] Cypress Semiconductor Corporation, "PSoC®5: CY8C55 Family Data Sheet," CY8C55 datasheet, Jun. 2011.

[20] A. Fujimoto, T. Kikugawa, and T. Lim, "CubeSat Stackable Interface," Internal Report, Univ. of Hawaii, Spring 2008.

[21] C. Clark, A. Strain, and A. L. Mazarias, "A high performance, very low cost power system for microspacecraft," *Proc. Euro. Space Power Conf.*, Konstanz, Germany, Sep. 2008.

[22] C. Clark, "An advanced electrical power system for CubeSats," *Proc. Euro. Small Sat. Services Symp.*, Madeira, Portugal, Jun. 2010.